Supporting Information

Stacking of MoS_2 monolayers by sequential electrochemical thinning of bulk crystals

Isaque A. A. Feitosa[a,b], Renan G. de Assis[a,b], Matheus F. F. das Neves[a], Leonardo H. Hasimoto[a,b], Alisson R. Cadore[a,c], Ingrid D. Barcelosd, Murilo Santhiago[a,b] *

[a] Brazilian Nanotechnology National Laboratory (LNNano), Brazilian Center for Research in Energy and Materials (CNPEM), Campinas, São Paulo 13083-970, Brazil

[b] Federal University of ABC, Santo André, São Paulo 09210-580, Brazil

[c] Programa de Pós-Graduação em Física, Instituto de Física, Universidade Federal de Mato Grosso, Cuiabá 78060-900, Mato Grosso, Brazil

[d] Brazilian Synchrotron Light Laboratory (LNLS), Brazilian Center for Research in Energy and Materials (CNPEM), Campinas, São Paulo 13083-970, Brazil

*e-mail: murilo.santhiago@lnnano.cnpem.br

Microelectrode fabrication and random flake transfer

The thin film-based microelectrodes were prepared by depositing 20 nm and 30 nm of Ti and Au, respectively, onto glass slides using an electron-beam system (AJA International). Before transferring the MoS_2 flakes, the microelectrodes underwent a cleaning sequence with acetone, isopropanol, and DI water in an ultrasonic bath for 5 min each. The cleaning procedure was completed by subjecting the microelectrodes to oxygen plasma (Diener Nano) at a power of 30%, pressure of 0.3 mbar, and temperature of 100 °C for 10 min. After cleaning the microelectrodes, bulk MoS_2 was exfoliated using the scotch tape method and transferred to the gold (Au) microelectrodes, applying acetone on the back face of the adhesive tape. Following the MoS_2 transfer, the microelectrodes were cleaned in acetone, 2-propanol, DI-water (room temperature), and hot DI-water (100 °C), then dried with nitrogen.

Stacking of MoS_2 monolayers through sequential electrochemical thinning (eTH)

Bulk MoS_2 was mechanically exfoliated and transferred onto Au microelectrodes, followed by sequential electrochemical thinning and vertical stacking of MoS_2 monolayers. MoS_2 crystals are first exfoliated by micromechanical cleavage using Nitto-tape on Ti/Au substrates, as described above. This is followed by an electrochemical process consisting of an initial chronoamperometric step at 1.5 V vs. Ag/AgCl, followed by ten cyclic voltammetry scans between –0.1 V and +0.5 V at a scan rate of 10 mV s^{-1} in a 0.5 mol L^{-1} H_2SO_4 solution.[1,2] Electrochemical thinning was performed using a conventional three-electrode configuration comprising an Ag/AgCl as reference electrode, a glassy carbon counter electrode, and the Au/bulk-MoS_2 microelectrode as the working electrode. MoS_2 thinning was conducted using a PGSTAT-302N potentiostat model from AUTOLAB (Eco Chemie, Netherlands), interfaced with a computer and controlled by the NOVA 2.8 software. Upon completion, the sample is dried under a nitrogen stream. This procedure enables controlled electrochemical thinning of MoS_2, resulting in the formation of monolayers with typical lateral dimensions on the order of 200 - 300 µm.

For stacking adjacent layers, a dry-transfer technique was employed, as described[3], using a commercial HQ Graphene transfer system. Bulk-MoS_2 flakes were picked up from Si/SiO_2 substrates using a polycarbonate (PC) membrane supported on a polydimethylsiloxane (PDMS) stamp at 100 °C. The selected flake was then aligned and

brought into contact - using XYZ micromanipulators at 180 °C - with the pre-exfoliated monolayer (homobilayer) MoS_2 region on the Au microelectrode. After the transfer, the structure was sequentially cleaned with chloroform, ethanol, and DI-water, followed by drying under nitrogen flow. Subsequently, the electrochemical thinning cycle was repeated to ensure complete removal of PC residues and to improve the layered architecture. This procedure was iterated at least three times to obtain vertically stacked MoS_2 monolayers.

Characterization

Raman and Photoluminescence (PL) spectra were acquired using a XploRA Plus Horiba equipment with a 532 nm laser and 50x objective lens. For the Raman (PL) measurements, each spectrum was collected during 15 (5) seconds and averaged with 5 (5) acquisitions. For data presentation, Raman spectra were normalized to the intensity of the most intense Raman mode (A_{1g}), while PL spectra were normalized with respect to the maximum intensity of the A exciton emission band. X-ray photoelectron spectroscopy (XPS) was carried out with a Thermo Scientific spectrometer (U.K.) using an Al Kα X-ray source (1486 eV). Survey scans and high-resolution Mo and S scans were collected at 1.00 and 50.0 eV pass energy, respectively. Optical images were taken using a Zeiss Microscope ICc5 at different magnifications. Scanning electron microscopy (SEM) images were obtained using a Quanta 650 FEG (Thermo Fischer Scientific) operating at 2 kV with a secondary electron detector. Topographic images were obtained in a ParkSystems NX10 atomic force microscope (AFM) in tapping mode. A NanoWorld FMR probe equipped with a Si tip with a nominal spring constant of 2.8 N m^{-1}, a nominal resonance frequency of 75 kHz, and 8.0 – 10.0 nm tip-end radius was used for the scanning. The AFM platform was mounted in an environmental chamber, which allows control over the relative humidity and temperature (10% and 25 °C).

S1) Influence of electrochemical parameters on the electrochemical thinning (eTH) of MoS_2

The influence of electrochemical parameters on the electrochemical thinning (eTH) process has been previously investigated by our research group[1] (Figure S1a-f), which provides a systematic analysis of the electrochemical thinning behavior of MoS_2 flakes under similar experimental conditions. In that study, cyclic voltammetry experiments (Figure S1a-b) showed that the presence of MoS_2 introduces a pronounced oxidation peak around ~1.5 V, which progressively decreases during successive cycles as the thinning process advances. Optical microscopy images obtained before and after electrochemical thinning were analyzed through image processing to quantify the thinned area (Figure S1c-d). By converting bulk and thinned regions into binary contrast (Figure S1c), the authors were able to estimate the fraction of thinned material under different electrochemical conditions.

The results demonstrate that applied potential strongly influences thinning efficiency. When 1.0 V vs. Ag/AgCl is applied, thinning occurs mainly at the flake edges, resulting in limited conversion (<10%). As the potential increases, the thinned area increases significantly, reaching a plateau above ~90% at approximately 1.5 V (Figure S1d). In addition, thinning efficiency depends on the initial thickness of the MoS_2 flakes, with thinner flakes undergoing more rapid thinning, whereas thicker flakes require additional electrochemical cycles (Figure S1e-f).

In our current work, the electrolyte (H_2SO_4) concentration was chosen primarily to ensure sufficient ionic conductivity for efficient charge transfer during the eTH. Therefore, a concentration of 0.5 mol L^{-1} was employed throughout the experiments. Electrolyte concentrations from 0.1 to 0.5 mol L^{-1}, typical in many electrochemical experiments, can be used for eTH of MoS_2 flakes.[4,5] If low concentrations are necessary for a specific experiment, we would recommend performing the experiment using microelectrodes to minimize iR drop.

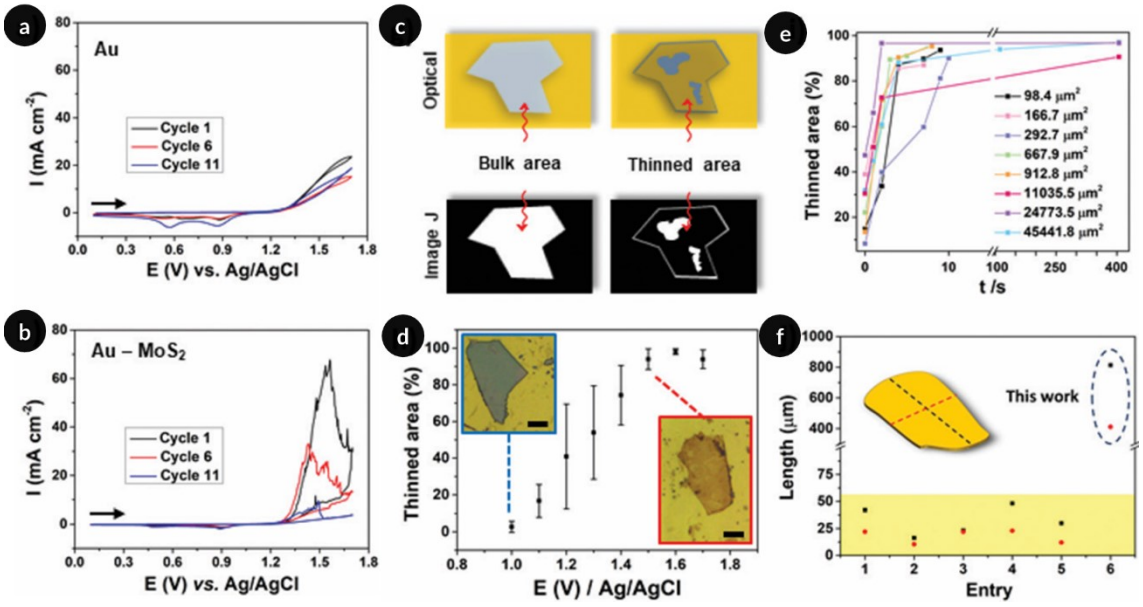

Fig S1. Cyclic voltammograms (CVs) obtained for (a) Au and (b) Au–MoS_2 (MoS_2 thickness = 345 nm) electrodes in 0.5 mol L^{-1} H_2SO_4 at 50 mV s^{-1}. The current was normalized by the geometric area of the electrodes. The area and thickness of the MoS_2 flake are 19 714 μm^2 and 345 nm, respectively. (c) Scheme illustrating the treatment by image J software. (d) Influence of the applied potential on thinned area. Scale bars are 25 μm. (e) Thinned area versus time. (f) Comparison of lateral flake sizes with different works in literature. Red and black dashed lines represent width and length, respectively. Adapted with permission from ref. [1]. Copyright 2022, Royal Society of Chemistry.

S2) Thickness-dependent and anisotropic electrochemical thinning (eTH) of MoS_2 flakes

The efficiency of electrochemical thinning (eTH) of MoS_2 is strongly dependent on the initial thickness of the crystals and their adhesion to the Au substrate. In our approach, more than 90% of thick crystals that are well adhered to the substrate undergo basal plane thinning until reaching the monolayer regime.[1]

This behavior is consistent with previous reports indicating that anodic dissolution of MoS_2 is thickness-dependent, with the dissolution rate increasing exponentially as the number of layers decreases.[6] Additionally, the process is kinetically anisotropic, typically progressing from the crystal edges toward the center.

A similar kinetic trend is observed in our system. Crystals with initial thicknesses in the range of ~60–150 nm exhibit highly efficient and uniform thinning. In contrast, thicker crystals (~300–500 nm) also undergo basal plane thinning down to the monolayer limit but require longer treatment times. In these cases, residual bulk-like regions are frequently observed at the crystal edges, reflecting intrinsic kinetic limitations and the anisotropic nature of the dissolution process.

This thickness-dependent behavior is illustrated in Fig. S2i-vi, which presents optical microscopy images of MoS_2 flakes with different initial thickness after eTH (Fig. S2i-iii), along with their corresponding Raman maps (Fig. S2iv-vi).

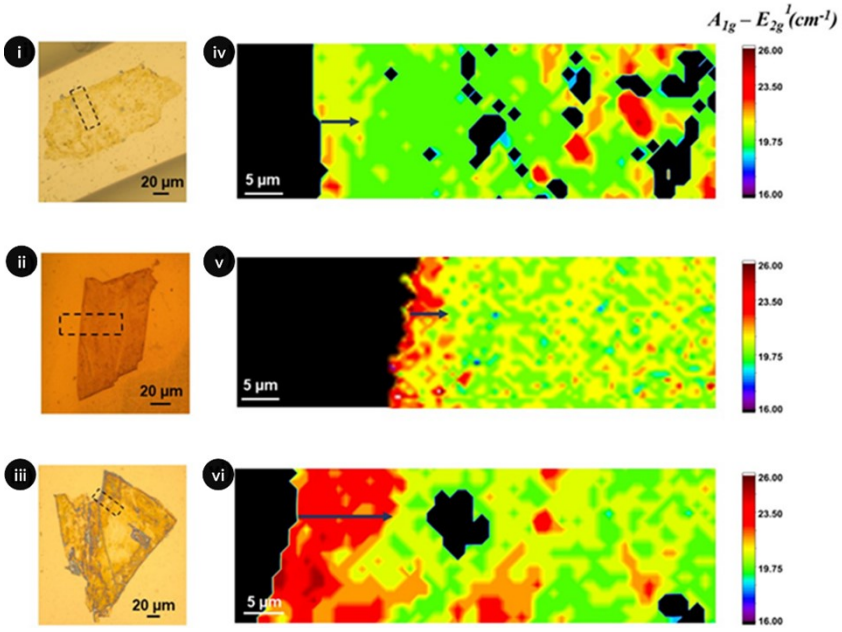

Fig S2. (i - iii) Optical microscope images of the electrochemically thinned flakes and their respective Raman maps (iv – vi). The thicknesses of the bulk flakes before the thinning process was 60 nm (i), 143 nm (ii) and 480 nm (iii). Adapted with permission from ref. [1]. Copyright 2022, Royal Society of Chemistry.

S3) Quantitative determination of monolayer area after electrochemical thinning (eTH)

The fraction of monolayer area obtained after electrochemical thinning (eTH) can be quantitatively determined through a combination of Raman mapping and image analysis. To further quantify the thickness-dependent efficiency of the eTH described in section S2, Raman micro-spectroscopy was employed to assess the thickness distribution across the flakes, following approaches previously reported in the literature.[6] In addition, the analysis below is based on data adapted from our previous report.[1] Specifically, the frequency difference between the A_{1g} and E^1_{2g} vibrational modes was mapped over the surface of the electrochemically thinned crystal. In the monolayer regime, this peak separation is typically observed in the range of ~18–20 cm^{-1}, enabling clear identification of monolayer regions.

This analysis is illustrated in Figure S3a-c, which presents optical microscopy images of MoS_2 flakes before and after eTH, along with the corresponding Raman data (Fig. S3d). Optical contrast combined with Raman mapping allows reliable distinction between bulk-like and monolayer regions across the flake surface. The representative flake shown in Fig. S3a-d was used for quantitative analysis, while an additional, thicker flake is presented in Fig. S3e-g. In this latter case, a similar thinning behavior is observed, with efficient basal plane conversion and residual bulk-like regions predominantly localized at the flake edges, further supporting the thickness-dependent and anisotropic nature of eTH.

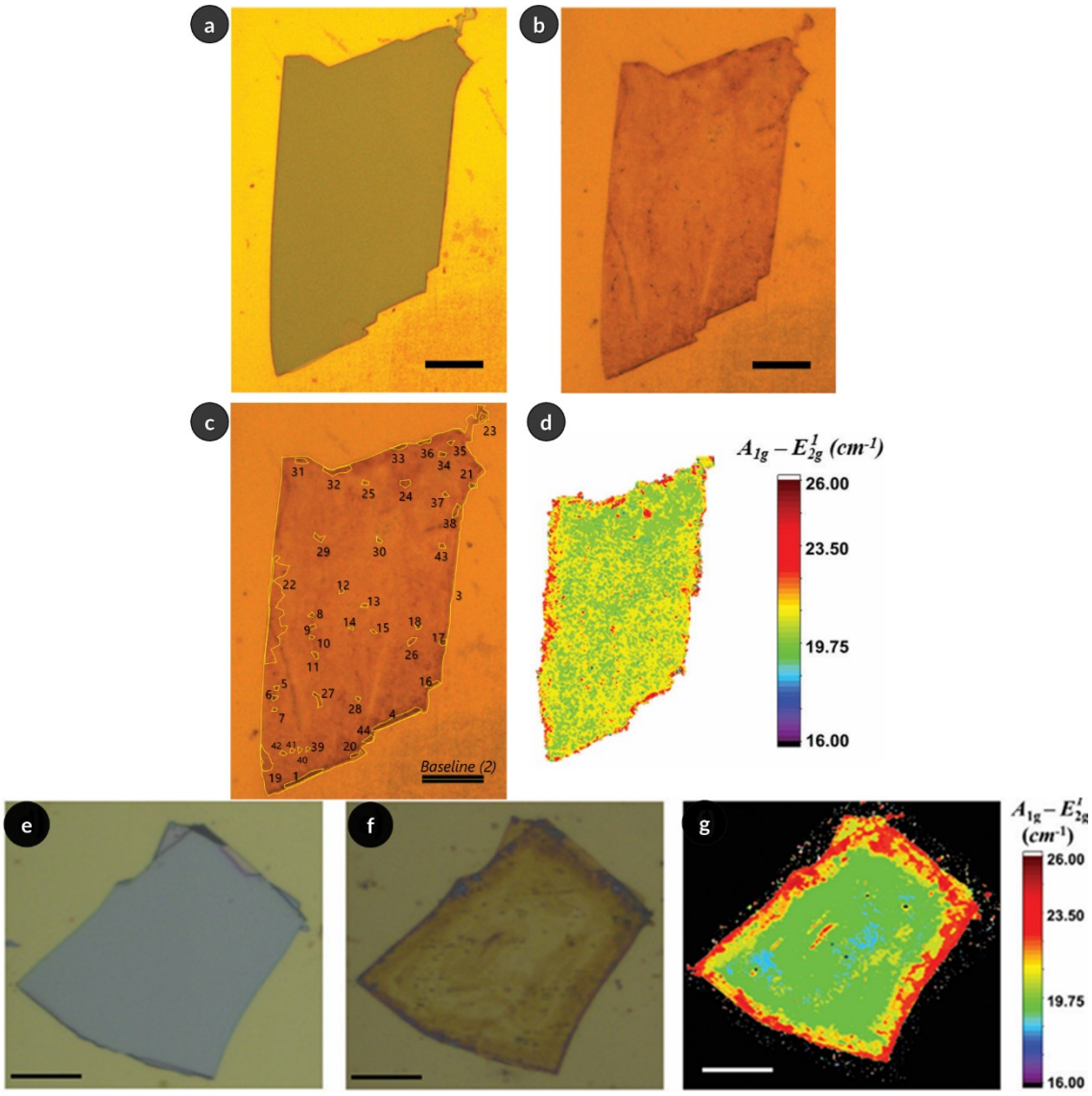

Fig S3. Optical (a, b, c) images of MoS_2 flakes before (a) and after (b, d) eTH. Scale bars are 20 µm. (c) Treatment by ImageJ software identifying the bulk and monolayers regions. (d) Raman spectra of bulk and monolayers regions (e, f) Optical images of a thicker MoS_2 flake before (e) and after (f) eTH. (g) Corresponding Raman map showing the thickness distribution. Scale bars are 20 µm. Adapted with permission from ref. [1]. Copyright 2022, Royal Society of Chemistry.

Quantitative image analysis was performed using ImageJ software by comparing optical images of the same flake before and after eTH (Fig. S3a-b). Spatial calibration was first validated using the scale bar (Fig. S3c, baseline, *measurement 2*), yielding a measured value of 19.848 µm, in close agreement with the nominal 20 µm, thereby confirming the accuracy of the calibration (Table 1).

Table 1. Spatial calibration of ImageJ software measurements using the scale bar in the Fig. S3c (after eTH).

Measurement	Description	Length / µm
2	Scale bar	19.848

Following calibration, the total flake area was determined via polygonal selection (Fig S3c). As summarized in Table 2, the total flake area corresponds to 5931.428 µm^2 (defined as 100%). Bulk-like regions were identified based on optical contrast and morphology and individually quantified.

Table 2. Area measurements of the total flake and a representative bulk-like region obtained from ImageJ in Fig. S3c (after eTH).

Measurement	Description	Area / µm^2
3	Total flake area	5.931.428
1	Bulk region	18.457
4-44	Bulk regions	*See table 3*
∑ (1 + 4-44)	Total bulk area	337.462

A detailed breakdown of all identified bulk-like regions (Fig. S3c, *measurements 4–44*) is provided in Table 3, where each region was individually quantified to ensure accurate determination of the residual bulk fraction.

Table 3. Area measurements of bulk-like regions (Measurements 4–44) obtained from ImageJ in Fig. S3c (after eTH).

Measurement	Area / µm²
1	18.457
4	30.900
5	2.204
6	2.847
7	1.882
8	1.928
9	3.030
10	1.653
11	3.696
12	2.525
13	2.571
14	1.102
15	1.561
16	5.142
17	4.201
18	2.640
19	19.995
20	3.742
21	3.145
22	124.242
23	5.372
24	6.887
25	3.191
26	4.821
27	7.277
28	2.112
29	5.487
30	2.479
31	5.923
32	15.978
33	5.188
34	3.558
35	2.479
36	4.293
37	2.479
38	6.657
39	1.309
40	1.699
41	1.653
42	2.548
43	3.099
44	5.510
∑ (1 + 4-44) *Total bulk area*	337.462

The cumulative bulk-like area, obtained by summing all contributions listed in Tables 2 and 3, corresponds to 337.462 µm^2. By directly comparing this value with the total flake area (Table 2), a residual bulk fraction of 5.69% is obtained, indicating that approximately 94.31% of the flake surface corresponds to monolayer basal plane after electrochemical thinning. The remaining bulk-like regions are predominantly localized at the flake edges, whereas the central region is largely converted into monolayer, consistent with the contrast observed in the corresponding Raman map (Fig. S3d,g).

This quantitative result is consistent with the thickness-dependent and anisotropic nature of the electrochemical thinning process discussed in section S2, as well as with previous observations reported in our previous work.[1]

S4) Extension of Electrochemical Thinning Beyond Conductive Electrodes

To illustrate that the electrochemical thinning process can also extend beyond the conductive region, conductive tracks (Ti/Au) were patterned on Si/SiO_2 substrates, followed by the transfer of bulk MoS_2 crystals onto the patterned surface. The electrochemical thinning process was then performed while maintaining partial electrical contact between the flake and the Au electrode. As shown in Figure S4a-b, the reduction of the layer number can also be achieved in regions located on the insulating Si/SiO_2 substrate adjacent to the electrode. Raman spectroscopy was used to assess the number of layers on these regions. As observed in Figures S4c–d, the spectra show a separation of approximately 19–20 cm^{-1} between the characteristic Raman modes, confirming that electrochemical thinning down to ML also occurs in insulating regions located next to the electrode.

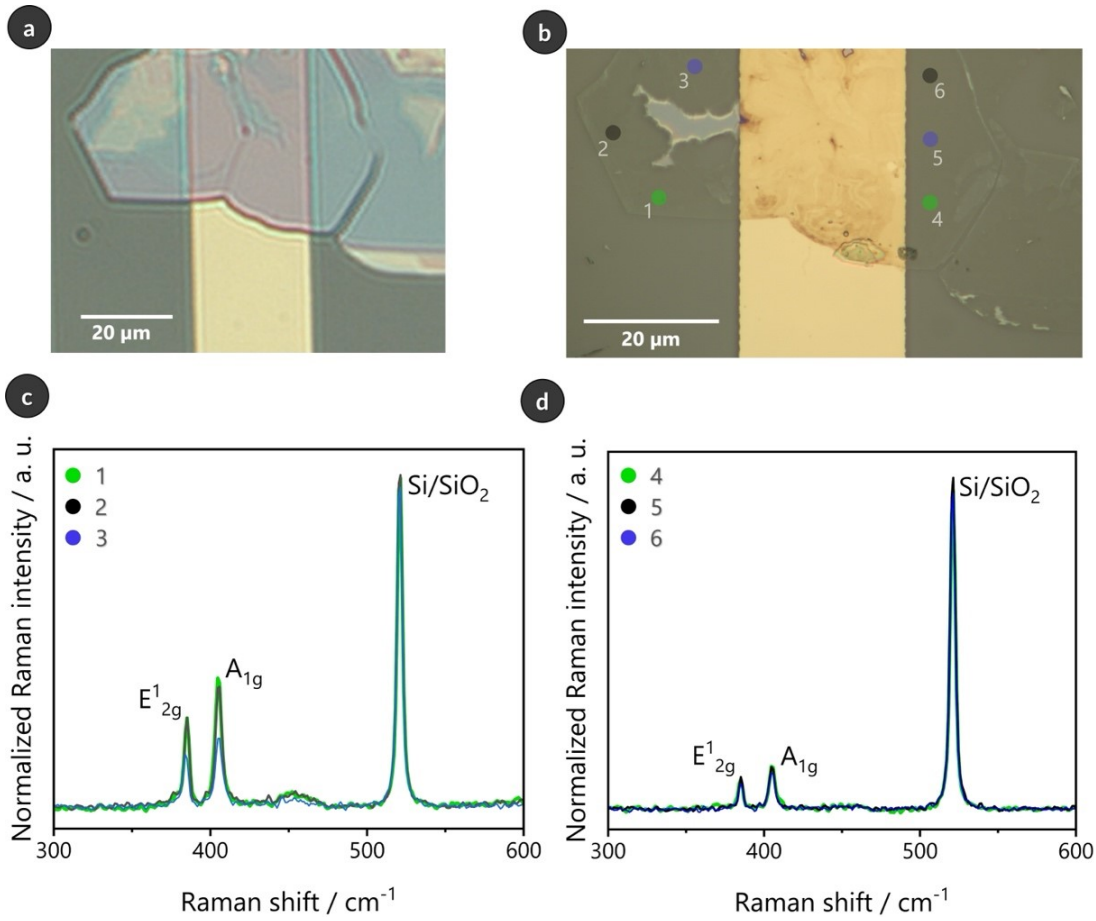

Fig. S4. Optical (a, b) images of MoS_2 flakes before (a) and after (b) eTH on the Si-SiO_2 substrate and corresponding Raman spectra of the MoS_2 flake on the Si-SiO_2 (c, d) substrate in different regions (1-6). The colored markers indicate the measurement positions, where points 1–3 (left side) and 4–6 (right side) correspond to the Raman spectra shown in panels (c) and (d), respectively. The color coding reflects the relative Raman intensity at each location: green denotes the highest intensity (used as the reference for normalization using the A_{1g} mode).

S5) SiO_2/bulk-MoS_2 substrate

Fig. S5 shows the optical image of the selected bulk MoS_2 transferred to the silicon substrate that was subsequently submitted to the controlled stacking and sequential electrochemical thinning. The bulk MoS_2 flake below was precisely transferred to Au electrodes, as shown in Fig. 3a.

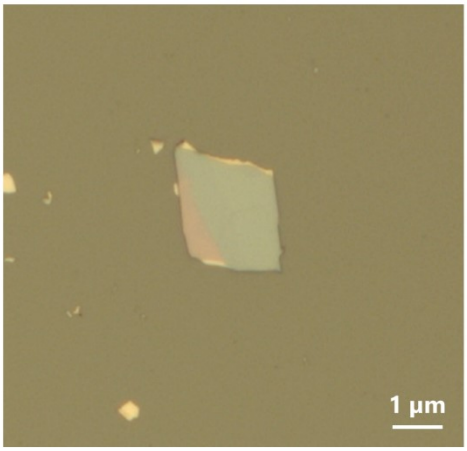

Fig. S5. Optical image of the MoS_2 selected flake transferred onto a silicon substrate.

S6) Au contact dependence for MoS_2 electrochemical thinning

Fig. S6i-vi shows the schematic electrochemical thinning process of bulk MoS_2 flakes. Note that in the third transfer process, a bulk MoS_2 flake is adsorbed in the center of the basal plane (Fig. S6-v), without any direct interface with the Au electrode. This situation must be avoided to prepare large thinned areas. Thus, we ensure the MoS_2 flake partially interfaces with the Au electrode during the third transfer, as shown in Fig. 3.

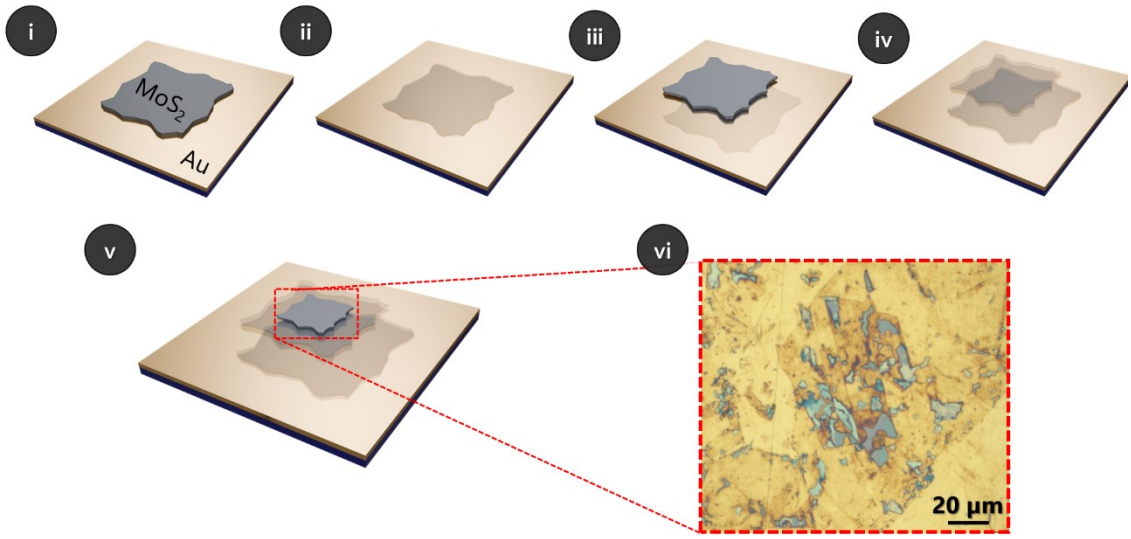

Fig. S6. Illustration of the sequential electrochemical thinning (eTH) of MoS_2 flakes on Au substrate. i) Bulk MoS_2 flake. ii) First eTH process. iii) Transfer of second bulk MoS_2 flake. iv) Second eTH process. v) Transfer of the third bulk MoS_2 flake. vi) Stereomicroscope image of the third bulk MoS_2 flake after the electrochemical thinning process.

S7) Area measurements

Fig. S7a-b illustrates the measurements performed by Image J software for the electrochemical thinned area of MoS_2 assembly. The overlapped area illustrated in Figure S7a was subtracted from the marked area shown in Fig. S7b to obtain the total area without bulk contributions. The total overlapped area was 546.33 μm^2.

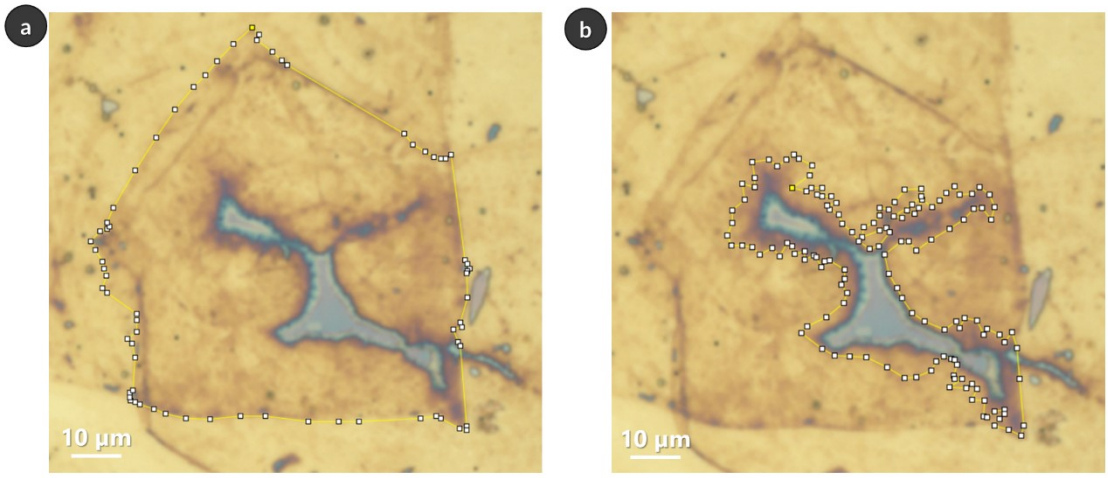

Fig. S7. a) Measurement for the thinned area of three stacked MoS_2 monolayers, and b) Measurement for the bulk region.

S8) Raman mapping of stacked MoS_2 layers

Raman mapping was performed to evaluate the spatial uniformity and layer-dependent properties of the stacked MoS_2 after sequential electrochemical thinning (eTH). Fig. S8a shows the optical image of the mapped region, while Figure S8b presents the spatial distribution of the frequency difference between the A_{1g} and E^1_{2g} Raman modes. The mapped region exhibits variations in the peak separation, with values approaching those expected for monolayer MoS_2 in specific areas. This behavior indicates that the electrochemical thinning process leads to locally well-defined monolayer-like regions within the stacked structure. Importantly, the presence of regions with reduced A_{1g}-E^1_{2g} separation supports the Raman and photoluminescence results discussed in the main text, reinforcing the interpretation of weak interlayer coupling and electronic decoupling between stacked layers.

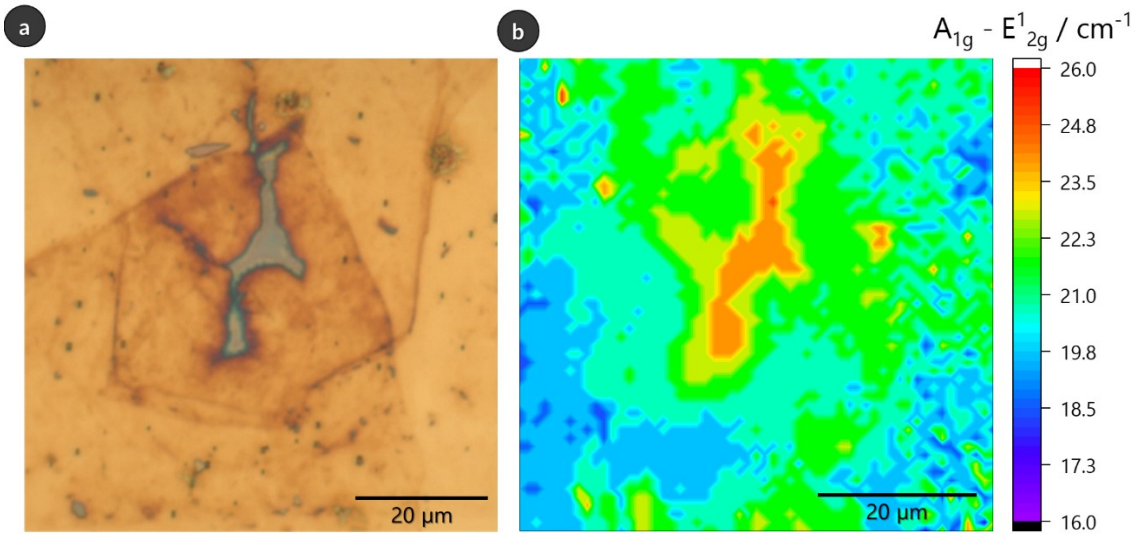

Fig. S8. Optical (a) image of three stacked MoS_2 monolayers after 3rd eTH and (b) Raman map of the three stacked MoS_2 monolayers.

S9) Atomic Force Microscopy (AFM)

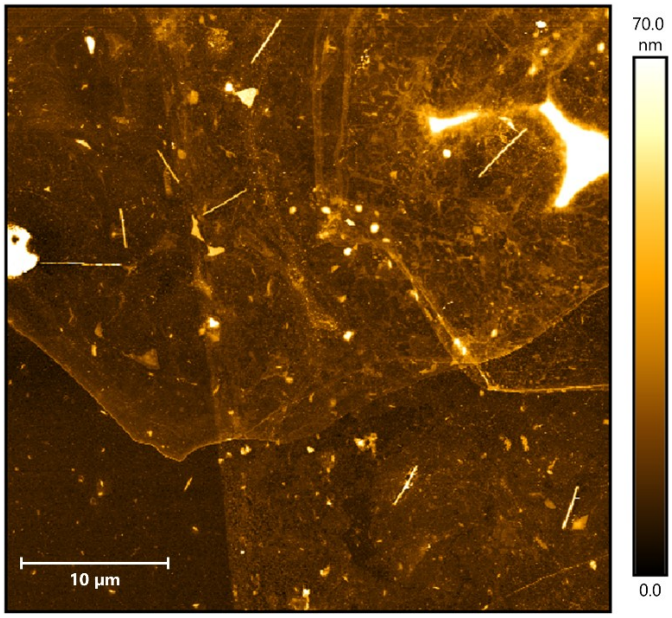

Fig. S9. AFM image for the thinned area of three stacked MoS_2 monolayers.

S10) XPS analysis of the disappearance of apical/bridging sulfur coordination during sequential eTH stacking

The apparent disappearance of these components after the third eTH step may be attributed to two factors. First, XPS is a surface-sensitive technique, probing only the uppermost few nanometers of the material. As additional MoS_2 layers are stacked, the surface probed by XPS corresponds primarily to the outermost layer, which may not contain the same sulfur configurations generated in earlier eTH cycles. Second, the electrochemical environment may promote the removal or reorganization of these sulfur species, possibly through dissolution or surface cleaning processes. This interpretation is supported by the high-resolution Mo 3d spectra, where the fraction of Mo^{6+} decreases from 2.7% in the final layer to 2.0 % for two stacked layers and 0.7 % for the first monolayer, suggesting that surface oxidation and associated sulfur species are progressively reduced during the stacking process.

References

1 N. De Freitas, B. R. Florindo, V. M. S. Freitas, M. H. D. O. Piazzetta, C. A. Ospina, J. Bettini, M. Strauss, E. R. Leite, A. L. Gobbi, R. S. Lima and M. Santhiago, Nanoscale, 2022, 14, 6811–6821.

2 B. R. Florindo, L. H. Hasimoto, N. De Freitas, G. Candiotto, E. N. Lima, C. De Lourenço, A. B. S. De Araujo, C. Ospina, J. Bettini, E. R. Leite, R. S. Lima, A. Fazzio, R. B. Capaz and M. Santhiago, J. Mater. Chem. A, 2023, 11, 19890–19899.

3 A. R. Cadore, B. L. T. Rosa, I. Paradisanos, S. Mignuzzi, D. De Fazio, E. M. Alexeev, A. Dagkli, J. E. Muench, G. Kakavelakis, S. M. Shinde, D. Yoon, S. Tongay, K. Watanabe, T. Taniguchi, E. Lidorikis, I. Goykhman, G. Soavi and A. C. Ferrari, 2D Mater., 2024, 11, 025017.

4 N. Liu, P. Kim, J. H. Kim, J. H. Ye, S. Kim and C. J. Lee, ACS Nano, 2014, 8, 6902–6910.

5 M. Zhao, C. Casiraghi and K. Parvez, Chem. Soc. Rev., 2024, 53, 3036–3064.

6 Justin R. Toole and Justin B. Sambur, J. Electrochem. Soc., 2023, 170, 116501.